Pre-Print Manuscript
Post-Print published in: Engineering Structures, Vol. 233, 15 April 2021
https://doi.org/10.1016/j.engstruct.2021.111890

Influence of Alkali-Silica Reaction (ASR) on Aggregate Interlock in Reinforced Concrete

Fiset M.[a], Sanchez. L. F. M.[b], Bilodeau. S.[c] , Mitchell D.[d], Bastien J.[e]

(a) Assistant Professor – Université du Québec à Chicoutimi, Department of applied sciences, 555 boul. de l'Université, Saguenay (Québec), G7H 2B1, Canada, Mathieu_fiset@uqac.ca (Corresponding author)

(b) Associate Professor – University of Ottawa, Department of civil engineering, Ottawa (Ontario), K1N 6N5, Canada, Leandro.sanchez@uottawa.ca

(c) M.Sc. – Université Laval, Département de génie civil et de génie des eaux, Québec (Québec), G1V 0A6, Canada, Sebastien.bilodeau@wsp.com

(d) Professor –McGill University, Department of Civil Engineering and Applied Mechanics, Montreal (Québec), H3A 0C3, Canada, Denis.mitchell@mcgill.ca

(e) Professor – Université Laval, Département de génie civil et de génie des eaux, Québec (Québec), G1V 0A6, Canada, Josee.bastien@gci.ulaval.ca

ABSTRACT:

Alkali-silica reaction (ASR) is one of the most damaging mechanisms affecting concrete structures worldwide. ASR effects on the durability and serviceability of damaged concrete are widely known and fairly well understood. However, the structural implications are still unclear, and a number of contradictory data are found in the literature, especially regarding shear behavior. The influence of ASR distressed reinforced concrete on aggregate interlock is presented in this paper. Push-off specimens having different reinforcement ratios were fabricated with ASR reactive coarse aggregates. The specimens were monitored over time and displayed different levels of expansion. Results indicated that ASR-induced expansion and damage were affected by the reinforcement ratio. However, little to no aggregate interlock reduction was observed on ASR-affected specimens up to moderate expansion levels. It was found that there were two controlling and competing mechanisms that affected aggregate interlock for ASR-affected specimens: the beneficial effects of chemical prestressing and the detrimental ASR-induced damage.

Key words: Aggregate interlock, Alkali-Silica Reaction (ASR), Shear behavior, Push-off test, Expansion.

1 INTRODUCTION

Alkali-silica reaction (ASR) is known as one of the most deleterious damage mechanisms for concrete. ASR is a chemical reaction between the alkali hydroxides from the concrete pore solution and some reactive siliceous phases from the aggregates [1-3]. ASR generates a product, the so

called alkali-silica gel, that swells in the presence of water, causing cracking and distress, which directly influences the concrete mechanical properties, especially the tensile strength and modulus of elasticity [1-3]. ASR effects on the durability and serviceability of affected concrete is widely known, while the structural implications on the long-term behavior is still unclear and a number of contradictory data are found in the literature, especially regarding the shear behavior of reinforced concrete elements affected by ASR.

1.1 Influence of ASR on the mechanical properties of affected concrete

Previous investigations have demonstrated that ASR has different effects on the mechanical properties of concrete such as the compressive strength, the tensile strength and the modulus of elasticity [4, 5]. Severe reduction in the tensile strength and the modulus of elasticity have been reported in literature while the compressive strength loss is typically less [4, 6]. These losses of tensile strength and modulus of elasticity at lower expansion levels seem to be linked to the formation of cracks within the aggregate particles. For higher levels of expansion, progression and interconnection of cracks within the cement paste seem to result in significant losses in the concrete compressive strength as well [1].

1.2 Influence of ASR on the structural behavior of affected structural members

Aspects of behavior of ASR affected structural elements that need further studies include: influence of cracking, loss of tensile and compressive strengths, loss of stiffness, influence of confinement effects (i.e., reinforcement ratio, external restraint), bond deterioration, aggregate interlock and the shear strength. It is well known that aggregate interlock has a strong influence on the shear strength (Figure 1). The concrete contribution to shear strength is due to both the tensile stresses in the diagonally cracked concrete and the aggregate interlock at the diagonal cracks [7-11]. This paper aims to understand the influence of ASR on aggregate interlock.

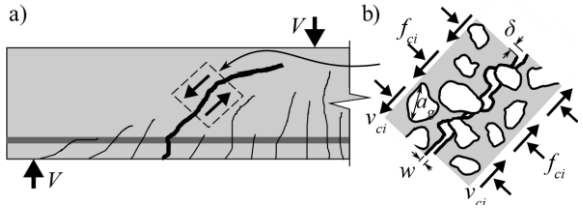

Figure 1: (a) Diagonal crack due to shear in reinforced concrete member and (b) close up of aggregate interlock at a crack

1.3 Aggregate interlock in reinforced concrete

Typically, push-off specimens with embedded stirrups (Figure 2a) are used to investigate aggregate interlock since the shear stress carry by this mechanism can be easily related to the crack width, w, and slip, δ, and the normal pressure at the crack interface, f_{ci}. By subtracting the dowel action of the stirrups from the total shear, V, the shear stress due to aggregate interlock, v_{ci}, can be determined as follows:

$$v_{ci} = \frac{V}{A_c} - \rho v_d \tag{1}$$

Where v_d is the shear stress in the reinforcement, A_c is the shear plane area and ρ is the reinforcement ratio. The normal pressure at the crack interface, f_{ci}, can be determined from the stirrups axial stress, f_s, as follows:

$$f_{ci} = \rho f_s \tag{2}$$

Walraven [12] carried out a large number of push-off tests (Figure 2a) and proposed an aggregate interlock model (Figure 2b). As illustrated in Figure 1b, aggregate interlock mechanism comes from the micro-roughened contact between the aggregate particles and the cement paste. The opening, w, and sliding, δ, of a crack causes bearing of aggregates with the surrounding cement paste (Figure 2b). This bearing results in a shear stress, v_{ci}, and a normal stress, f_{ci}, acting perpendicularly to the crack plane. Thus, this aggregate interlock mechanism is directly related to the size, shape, amount and mechanical characteristics (i.e., stiffness, strength, hardness) of the coarse aggregate and cement paste as well as the amount of reinforcement crossing the crack. Increasing the crack width, w, or reducing the aggregates size, a_g, reduces the contact area between the aggregates and cement paste, which reduces the aggregate interlock. Increasing the concrete compressive strength enhances the bearing capacity of the aggregate-cement paste interface, which improves the aggregate interlock. However, the use of high-strength concrete (compressive strength measured on cylinder, f_c', larger than 60 MPa) or concrete with weak aggregates can significantly reduce aggregate interlock because aggregate particles may fracture under stress at the crack [13-16].

By assuming a rigid-plastic stress-strain relationship between the aggregates and the surrounding material matrix, the following equations were proposed to determine the aggregate interlock shear stress, v_{ci}, and the resulting perpendicular stress, f_{ci} in normal strength concrete [12, 17].

$$v_{ci} = -0.04 f_c' + \left[1.8 w^{-0.80} + \left(0.292 w^{-0.707} - 0.25\right) f_c'\right] \delta \quad (3)$$

$$f_{ci} = -0.06 f_c' + \left[1.35 w^{-0.63} + \left(0.242 w^{-0.552} - 0.19\right) f_c'\right] \delta \quad (4)$$

These equations provide a relationship between the stress v_{ci} and f_{ci}, and the displacement at crack w and δ. This aggregate interlock model was validated by Walraven [12] as illustrated for the test specimen 1/0/6.8 in Figure 2c. When aggregates particles are expected to fracture under stress at cracks, that is for high-strength concrete or concrete with weak aggregates, Walraven et al. [13] and fib [17] recommends reducing v_{ci} and f_{ci} determined from Eq. (3) and (4) by 65%.

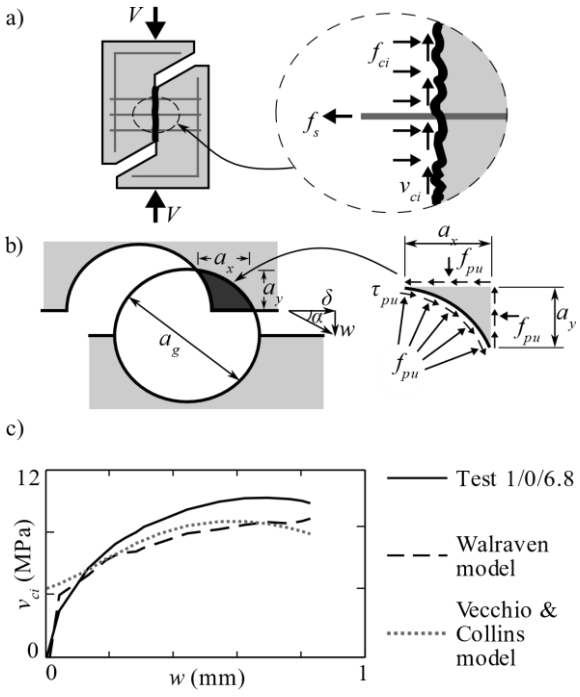

Figure 2: (a) Push-off test to investigate aggregate interlock, (b) Walraven aggregate interlock model and (c) comparison between analytical models and push-off test 1/0/6.8 carried out by Walraven [12]

Vecchio et al. [18] proposed a simplified model to determine aggregate interlock capacity based on the experiments carried out by Walraven [12]. This simplified model given by Eq. (5) can be

used to determine the interface shear stress at a crack due to aggregate interlock, v_{ci}, according to the compressive stress across the crack interface, f_{ci}, and a maximum aggregate interlock shear capacity, $v_{ci,max}$. This maximum aggregate interlock shear capacity given by Eq. (6) considers that a larger crack width reduces the contact area and the aggregate interlock capacity while the use of larger aggregates increases the contact area and the aggregate interlock capacity (see Figure 2). For high-strength concrete or concrete containing weak aggregates, the aggregates may fracture under stress and an aggregate size of 0 mm is suggested in Eq. (6) [19].

$$v_{ci} = 0.18 v_{ci,max} + 1.64 f_{ci} - 0.82 \frac{f_{ci}^{\ 2}}{v_{ci,max}} \tag{5}$$

$$v_{ci,max} = \frac{\sqrt{f_c'}}{0.31 + 24w/\left(16 + a_g\right)} \tag{6}$$

Figure 2c compares the prediction of one of Walraven's test specimens using Eq. (5). This simplified model provides a good prediction of the aggregate interlock shear stress as a function of the crack width. Due to its simplicity and accuracy, design codes are based on the model developed by Vecchio and Collins to determine the interface shear capacity due to aggregate interlock in reinforced concrete members [17, 20-22].

1.4 ASR effects on concrete properties

The behavior of aggregate interlock in ASR-affected concrete is a complex phenomenon. According to Blight et al. [23], Duthinh [24] and Yang et al. [25], ASR expansion tends to reduce shear crack openings of damaged concrete which would result in an additional aggregate interlock contribution. On the other hand, the reduction of concrete mechanical properties reduces the bond and bearing capacity between the aggregates and the cement paste reducing aggregate interlock capacity. Furthermore, it has been found that ASR might potentially cause distress within the aggregate particles, which may result in a decrease of aggregates interlock.

According to Sanchez et al. [6] ASR crack development in plain concrete (i.e., without reinforcing bars) under free expansion can be described in a two-step processes: a) first, crack formation happens within the reactive aggregate particles at low expansion levels (about 0.05% expansion) and; b) then these cracks extend into the cement paste, establishing important crack networks as the expansion level increases. Moreover, the authors proposed a qualitative damage model that

displays the crack types (Type A – sharp cracks; Type B – onion skin cracks) and their development as a function of ASR expansion for plain concrete (see Figure 3).

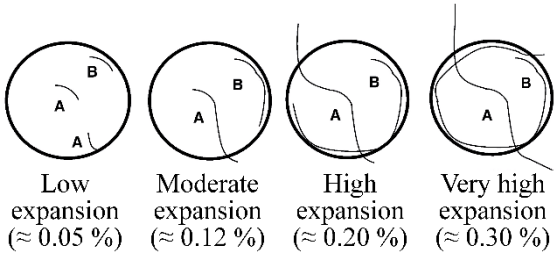

Figure 3**:** Qualitative ASR damage model as a function of expansion for plain concrete (adapted from Sanchez et al. [6])

2 SIGNIFICANCE OF ASR EXPANSION

To the authors' knowledge, no investigation has been carried out to investigate the influence of ASR on aggregate interlock with direct shear tests. A number of studies were conducted to assess the structural implications of ASR-induced expansion and damage in shear for shear critical members (Figure 1a) [26-29]. Some experimental studies showed an increase in shear capacity as a function of ASR development due to the so-called "chemical prestressing" mechanism (i.e., expansion of concrete due to ASR induces tension in the reinforcement causing compression across the shear crack interface [29-31]). On the other hand, other experimental investigations performed on ASR affected members (e.g., bridge decks) have demonstrated that the actual capacity found was only about 75% of the expected non-damaged members [30, 31]. It is clear that there is no general agreement on the effects of ASR on the shear capacity of affected members and hence further studies are needed.

3 METHODOLOGY

To investigate the effect of ASR on aggregate interlock, direct shear tests were carried out on reinforced concrete specimens containing highly reactive coarse aggregates. The responses of these specimens were studied at selected expansion levels.

3.1 Details of push-off specimens

Twenty-six push-off specimens were fabricated to investigate aggregate interlock in ASR affected concrete (see Figure 4 and Figure 5). Notches of 12.7 mm deep were made to ensure that the shear

plane was located at the center of the specimens over a height of 300 mm (see Figure 4b). The resulting shear plane area, A_c, is equal to 52380 mm².

A first series of two specimens, Series "0S", was reinforced with 10M reinforcing bars (bar diameter, d_b, of 11.3 mm and area, A_b, of 100 mm²) but did not contain any stirrups (specimens not illustrated in Figure 4). These two specimens were not used for push-off tests but were used to compare ASR-induced expansion. The other specimens were reinforced with 10M reinforcing bars and different amounts of closed 10M stirrups across the shear plane (see Figure 4). A second series of twelve specimens, Series "2S", was reinforced with two 10M closed stirrups (total stirrups area, A_s, of 400 mm²), which represent a reinforcement ratio, $\rho = A_s / A_c$, of 0.76%. A third series of twelve specimens, Series "4S", was reinforced with four 10M closed stirrups (A_s = 800 mm²), which represent a reinforcement ratio of 1.53%. Specimens of the series 2S and 4S were used for push-off testing as well as for ASR expansion monitoring.

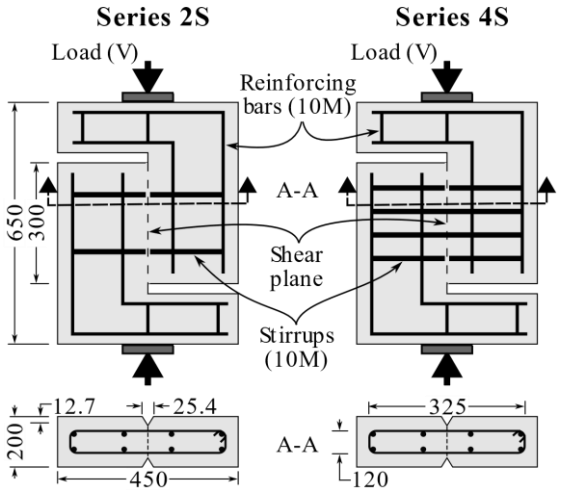

Figure 4: Push-off specimens of Series 2S and 4S with two and four stirrups, respectively (dimensions in mm)

3.2 Materials properties

Grade 400 [32] was used for the 10M reinforcing bars (Young modulus, E_s, of 200 000 MPa and measured yield strength, f_y, of 436 MPa). A 35 MPa concrete mixture enabling a fast ASR development in the laboratory was selected for this study. The coarse aggregates ranged from 5 to

20 mm in size (a_g = 20 mm in Eq. (6)). Non-reactive fine aggregate was used in combination with a highly reactive gravel from New Mexico, USA. The concrete mixture was made with a conventional (CSA Type GU, ASTM Type I) high-alkali (0.88% Na_2O_{eq}) Portland cement. Reagent grade NaOH was used to raise the total alkali content of the mixtures to 1.25% Na_2O_{eq}, by cement mass, for accelerating the expansion process due to ASR. Table 1 gives the detailed aggregate properties and Table 2 shows the concrete mix design.

Aggregate Identification			Rock Type Reactive rock types are in bold	Specific gravity (g/cm^3)	Absorption (%)	AMBT [1] 14d exp,%
Type	Reactivity	Designation (location)				
Coarse	Reactive	New Mexico (USA)	Polymictic gravel (**mixed volcanic, quartzite, chert**)	2.53	1.59	1.114
Fine	Non-reactive	Quebec (Canada)	Natural derived from granite	2.71	0.54	0.032

[1] Accelerated Mortar bar expansion at 14 days [33].

Table 1: Aggregates properties

Concrete Mix design	Ingredients	Materials (kg/m^3) Mixtures NM gravel	Materials (L/m^3) Mixtures NM gravel
Components	Cement	370	118
	Sand	714	264
	Coarse aggregate	1073	424
	Water	174	174
	Air	-	20.0
	Alkalis	4.63	-
	w/c	0.47	-

Table 2: Concrete mix proportions.

3.3 Concrete curing and ASR expansion measurement

The specimens were placed in the moist curing room immediately after casting for a 7-day curing period, after which they were demolded. Holes, 10 mm in diameter by 65 mm long, were drilled into each specimen (Figure 5a) and stainless steel gauge studs were installed, with fast-setting cement slurry, to measure the expansion perpendicular to the shear plane.

a)

b)

c)

Figure 5: (a) Push-off specimen used and stud locations for ASR expansion measurement, (b) storage of specimens in sealed plastic containers and (c) ASR measurement

The specimens were then stored in the laboratory for 48h at 23°C, after which the "0" length reading was performed and the specimens were placed in sealed plastic containers lined with damped burlap (2 specimens per container, Figure 5b). All containers were stored at 38°C and 100% R.H., and all the push-off specimens were monitored regularly for length variations (see Figure 5c). As per ASTM-C1293 [34], the containers were cooled to 23 °C for 16 ± 4 h prior to periodic expansion measurements.

To estimate the targeted ASR expansion for push-off specimens, the concrete expansion was monitored in the two specimens without stirrups (Series 0S). Then, expansion levels of 0.05% ± 0.01 and 0.12% ± 0.01% were selected for half of the push-off specimens of the series 2S and 4S. The push-off specimens reaching an expansion of 0.05% and 0.12% were designated as "R5" and "R12", respectively. These expansion levels were chosen according to desired ASR damage levels observed microscopically by Sanchez et al. [6]. Once these expansion levels were reached after a conditioning period of time, specimens were wrapped in plastic film and stored at 12°C to limit ASR progression until testing as described by Sanchez et al. [6].

For comparison, non-reactive concrete specimens designated as "NR5" and "NR12" were tested. These specimens were fabricated with the same mix-design and stored in similar conditions and the same conditioning period as the corresponding specimens R5 and R12, but lithium-based admixtures were used in the concrete mix to inhibit ASR development.

3.4 Loading procedure and measurements of push-off specimens

Prior to testing, the specimens were kept for 48h in the moist curing room to allow appropriate re-saturation [35]. Then the push-off test was carried out in the following two steps.

3.4.1 Pre-cracking phase

All the specimens were pre-cracked along the critical shear plane before push-off testing. Steel plates designed to fit the shear plane notches were placed under and over the notches and then loaded at a rate of 0.3 mm/min to create tensile stresses and cracking along the desired shear plane (see Figure 6). The pre-cracking phase was completed when the crack width measured by four linear variable differential transformers (LVDT) (two on each side of the critical shear section, see Figure 7a) reached a crack width of 0.10 mm.

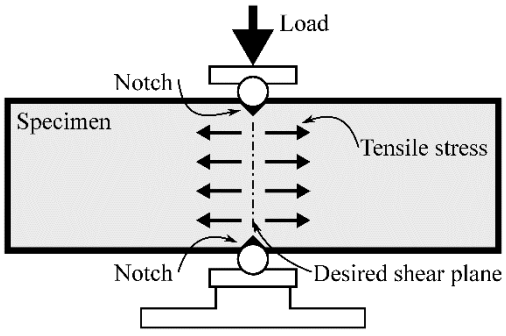

Figure 6: Pre-cracking of a push-off specimen

a) b)

Figure 7: (a) Measurements of crack width during pre-cracking phase by four LVDTs (two on each side) and (b) crack width and slip during push-off testing

3.4.2 Push-off testing

The four LVDTs used during pre-cracking remained on the specimen to measure crack width during push-off testing. In addition, two new LVDTs (1 per side, see Figure 7b) were installed to measure crack slip. The specimen was placed in the testing frame as illustrated in Figure 7b and then loading was applied at a rate of 0.25 mm/min. The test was considered completed when the average crack slip reached approximatively 2 mm, which is considered to be large enough to evaluate the aggregate interlock shear behavior [34].

4 ASR DEVELOPMENT ON THE CONCRETE SPECIMENS

Figure 8 presents representative values of expansion measured perpendicular to the shear plane (see Figure 5c). All the non-reactive concrete specimens 2S-NR and 4S-NR, due to the inclusion of lithium to control ASR expansion, showed very small expansion levels over time (i.e. generally

lower than 0.03%). The specimens with reactive concrete, 0S-R, 2S-R and 4S-R (without lithium), exhibited significant expansion. The reactive concrete specimen without reinforcement, 0S-R, reached 0.05% and 0.10% expansion at 9 and 16 weeks (64 days and 115 days), respectively. After 24 weeks (168 days), expansion reached a maximum value of 0.12%. A longer delay was observed for reactive concrete specimen with stirrups. The reactive concrete specimen with two stirrups, 2S-R, reached 0.05% and 0.10% expansion at 17 and 29 weeks (121 and 203 days), respectively. The reactive concrete specimen with four stirrups, 4S, reached 0.05% and 0.10% expansion at 19 and 45 weeks (133 and 321 days), respectively. After reaching 0.10% expansion, the rate of expansion slowed down and maximum values of 0.12% and 0.11% were reached after 53 and 57 weeks (371 and 399 days) for the representative specimens 2S-R and 4S-R presented in Figure 8, respectively. It is clear that increased confinement due to increasing the amount of stirrups delayed the measured expansion.

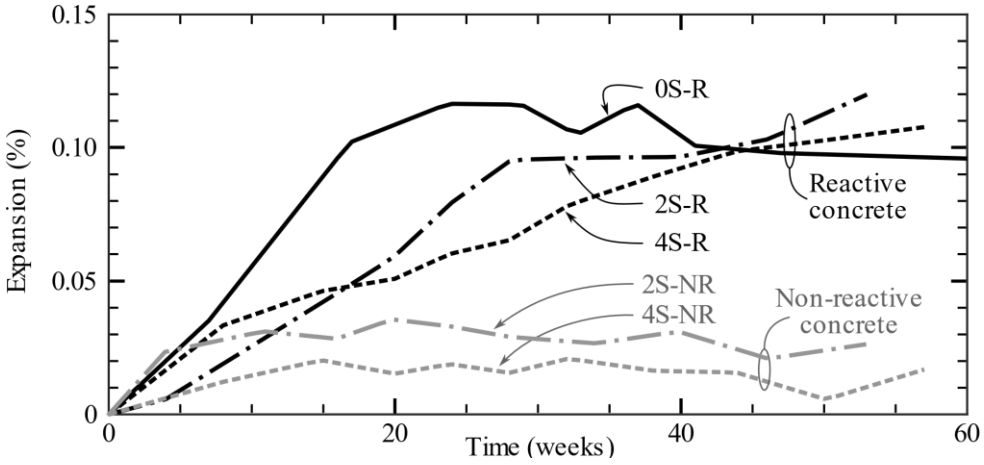

Figure 8: Typical values of ASR expansion as a function of time for reactive and non-reactive concrete specimens with different amounts of stirrups

5 PUSH-OFF TESTS RESULTS AND DISCUSSION

5.1 Test results

Figure 9 and Table 3 present the push-off test results for the reactive and non-reactive concrete specimens. Figure 9 shows the aggregate interlock shear stress, v_{ci}, the average shear stress due to dowel action of the stirrups, ρv_d, the crack width, w, and the compressive stress on the crack interface, f_{ci}, as a function of the crack slip, δ. These average values for each series were

determined for each value of slip. Table 3 compares the average peak values of aggregate interlock, $v_{ci,peak}$, and the corresponding compressive stress on crack interface, $f_{ci,peak}$, crack slip, δ_{peak}, and width, w_{peak}, for all the reactive and non-reactive concrete specimens. This table also presents the measured expansion levels at the time of testing each specimen.

The aggregate interlock shear stress was determined with Eq. (1) by taking the total shear stress, V / A_c, and subtracting the shear stress due to dowel action of the stirrups, ρv_d. The model proposed by Maekawa et al. [36] and Moradi et al. [37] was used to determine v_d. This model validated by several authors [37-41] considers interaction between the shear stress and the axial stress in the stirrups at a crack and can be expressed as:

$$v_d = \frac{12.1 f_c'^{0.6375} E_s^{0.25}}{d_b k_{di}^{3}} \delta \le \frac{f_y}{\sqrt{3}} \sqrt{1-\left(\frac{f_s}{f_y}\right)^4} \tag{7}$$

In this equation, f_s is the axial stress in the stirrups at a crack and k_{di} is a concrete damage parameter that considers the bar diameter, the crack width and slip. Considering an initial stirrup deformation caused by ASR, ε_{s0}, and an elastic strain-hardening stress-strain response, the stirrups axial stress, f_s, is determined from the crack opening as follows [42-44]:

$$f_s = \sqrt{\frac{2E_s f_c'^{2/3}}{d_b} w} + E_s \varepsilon \qquad w \le w_y \tag{8}$$

$$f_s = \sqrt{\frac{2E_h f_c'^{2/3}}{d_b}\left(w - w_y\right)} + E_h \varepsilon_{s0} + f_{yr} \qquad w > w_y \tag{9}$$

Where E_h is the strain-hardening modulus (taken as 1000 MPa), f_{yr} is a reduced yield strength that considers the effect of shear stress from Eq. (10) [36] and w_y is the crack width at the yielding of the stirrups given by Eq. (11).

$$f_{yr} = f_y \sqrt[4]{1-3\left(v_d / f_y\right)^2} \tag{10}$$

$$w_y = \frac{d_b E_s}{2 f_c'^{2/3}} \left(\frac{f_{yr}}{E_s} - \varepsilon_{s0}\right)^2 \tag{11}$$

The ASR-induced expansion of the specimens was measured 65 mm from the specimen surface and the initial stirrups strain, ε_{s0}, was taken equal to the concrete expansion at this location.

Test*		cure	Reactive concrete (R)						Non reactive concrete (NR)						R/NR	
			ε_{ASR}	f_c'	δ_{peak}	w_{peak}	$v_{ci,peak}$	$f_{ci,peak}$	ε_{ASR}	f_c'	δ_{peak}	w_{peak}	$v_{ci,peak}$	$f_{ci,peak}$	$\frac{v_{ci,peakR}}{v_{ci,peakNR}}$	$\frac{f_{ci,peakR}}{f_{ci,peakNR}}$
		weeks	%	MPa	mm	mm	MPa	MPa	%	MPa	mm	mm	MPa	MPa		
2S	5-1	39.9	0.029	42.6	0.20	0.17	8.87	2.46	0.009	45.0	0.22	0.14	8.32	1.99	1.07	1.23
	5-2	17.9	0.050	41.6	0.30	0.21	8.49	3.00	0.013	43.7	0.16	0.15	7.49	2.10	1.13	1.43
	12-1	46.1	0.088	42.7	0.24	0.29	9.58	3.45	0.018	45.1	0.26	0.15	6.92	2.20	1.38	1.57
	12-2	53.1	0.120	42.8	0.40	0.36	8.88	3.51	0.022	45.2	0.38	0.28	7.82	2.98	1.14	1.18
	12-3	53.1	0.139	42.8	0.45	0.47	8.62	3.56	0.027	45.2	0.28	0.24	7.90	2.85	1.09	1.25
Average				42.5	0.32	0.30	8.89	3.20		44.8	0.26	0.19	7.69	2.42	1.16	1.33
4S	5-1	28.0	0.049	45.2	0.18	0.13	9.81	5.12	0.013	47.1	0.26	0.23	11.74	5.31	0.84	0.96
	5-2	59.0	0.049	42.9	0.17	0.14	10.59	5.17	0.000	46.9	0.15	0.11	10.62	3.42	1.00	1.51
	5-3	23.9	0.059	45.0	0.51	0.47	10.52	6.92	0.008	46.9	0.17	0.12	10.77	3.75	0.98	1.85
	12-1	50.1	0.098	45.7	0.45	0.53	10.77	7.10	0.004	47.6	0.15	0.13	11.76	3.83	0.92	1.85
	12-2	57.1	0.108	45.8	0.29	0.46	12.12	7.09	0.017	47.7	0.26	0.21	12.13	5.20	1.00	1.36
	12-3	66.0	0.115	43.0	0.48	0.59	10.35	7.15	0.017	47.0	0.18	0.16	10.97	4.64	0.94	1.54
Average				44.4	0.38	0.44	10.87	6.69		47.2	0.18	0.15	11.25	4.17	0.94	1.51

* No result was monitor for the specimens 2S-5R-3 and 2S-5NR-3 due to the measuring system malfunction

Table 3: Summary of push-off test results for specimens with two and four stirrups

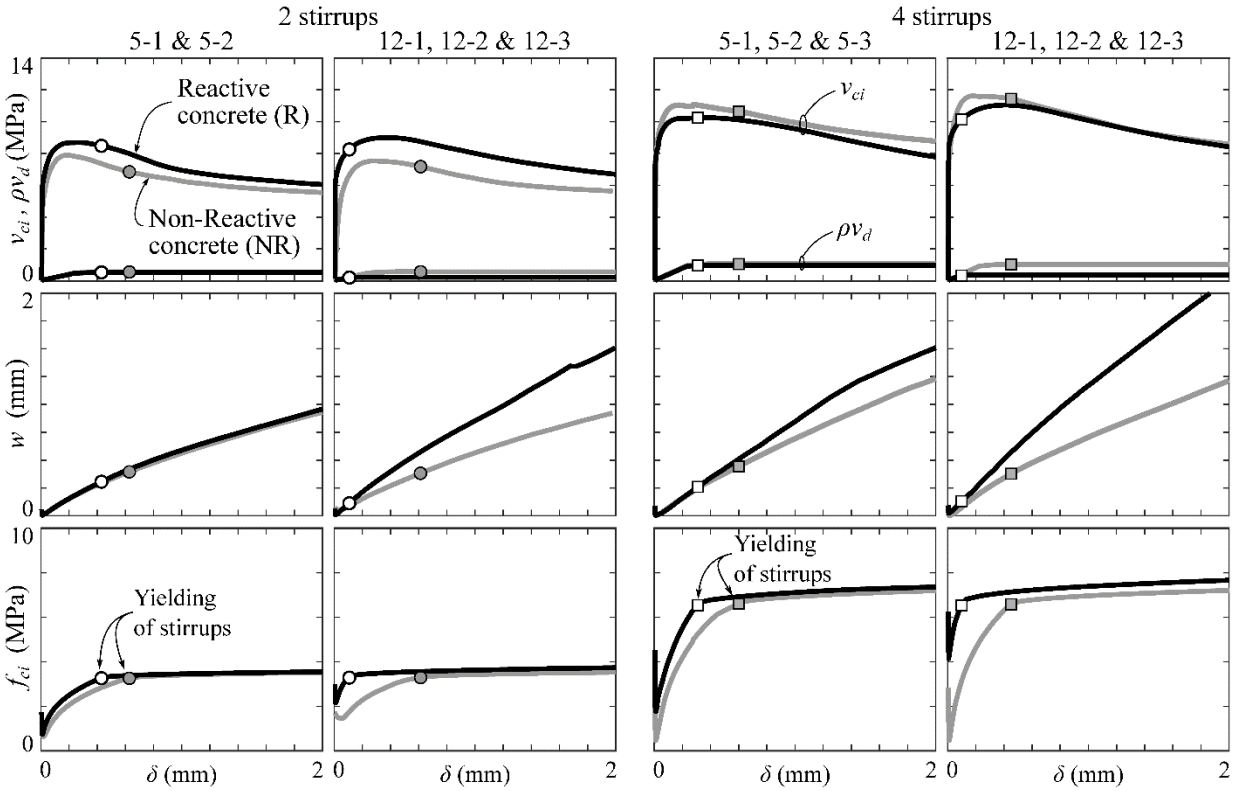

Figure 9: Average values of: shear stress at crack due to aggregate interlock, v_{ci}, dowel resistance, ρv_d, crack width, w, and the compressive stress on crack, f_{ci}, as a function of the crack slip, δ

5.2 Influence ASR-induced expansion level and amount of stirrups

It can be seen from Figure 9 that, before any shear was applied, the specimens exhibit a very small crack (less than 0.1 mm) due to precracking. This precracking caused tensile stress in the stirrups and an initial compressive stress on the crack interface, f_{ci}. ASR expansion levels induces additional tensile stresses in the stirrups (i.e. "chemical" prestressing) and increased compressive stresses on the crack interface. As the amount of stirrups and ASR expansion increase, this initial compressive stress on the crack interface applied by the stirrups increases. For example, the compressive stress on the crack due to chemical prestressing of the stirrups in the reactive concrete specimens with two stirrups, R5 and R12, reaches on an average 0.65 and 1.76 MPa, which represents 20% and 53% of the stirrup yield stress, respectively.

When shear is applied, the compressive stress on the crack interface applied by the stirrups tends to close the shear crack. For the same applied shear, the initial stress due to ASR chemical prestressing results in a smaller shear crack width than the specimens with non-reactive concrete. As the initial compressive stress on the crack interface increases, friction on the crack interface increases and a larger shear stress must be applied to start the shear crack opening and sliding. Thus, the initial slope of the shear stress versus slip curve in Figure 9 is steeper for the reactive specimens (R5 and R12) than the non-reactive ones (NR5 and NR12).

When crack slip occurs, the shear stress due to dowel action of the stirrups is engaged. However, it can be seen in Figure 9 that the shear stress carried by the stirrups, ρv_d, is relatively small compared to the aggregate interlock, v_{ci}. For Series 2S and 4S, the shear stress due to dowel action, ρv_d, reached an average 0.37 MPa and 0.62 MPa, respectively (see Figure 9) at the peak aggregate interlock shear stress. The shear stress due to dowel action represents less than 6% of $v_{ci,peak}$. At the end of the test, v_{ci} decreases and ρv_d represents less than 11% of v_{ci}.

When the applied shear increases, the aggregate interlock becomes fully engaged and the crack slips and opens. The relationship between the average crack width and the average crack slip is shown in Figure 10 for the push-off specimens. It can be seen in Figure 9 and Figure 10 that this crack displacement is similar for reactive and non-reactive concrete specimens up to the yielding of the stirrups. Yielding of the stirrups occurs at similar crack displacements for the specimens with two and four stirrups. However, increasing ASR reduces the crack width at stirrup yielding since the stirrups were in tension before shear was applied. On average, crack widths of 0.60 mm, 0.40 mm and 0.15 mm and crack slips of 0.30 mm, 0.25 mm and 0.10 mm were determined when the stirrups yielded for the specimens NR, R5 and R12, respectively.

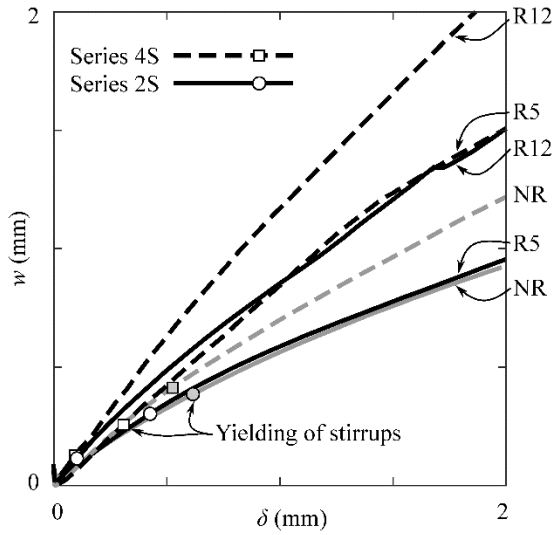

Figure 10: Average crack width, w, versus average crack slip, δ

After the stirrups reach yielding, the increase of crack width does not result in a significant increases of compressive stress at the crack interface, f_{ci}, and the crack opens (see Figure 9). Because the yielding of the stirrups occurs at smaller slips for the reactive concrete specimens, the crack width becomes larger for these specimens than for the non-reactive concrete specimen after stirrups yielding (see Figure 9 and Figure 10). Consequently, the peak-aggregate interlock generally occurs after yielding of the stirrups for the specimens with more significant ASR expansion. At the peak aggregate interlock, the specimens R12 with two and four stirrups reached on an average $f_{ci,peak}$ of 3.51 MPa and 7.11 MPa, respectively (see Table 3), which exceed the stirrups yielding. For the non-reactive specimens with two and four stirrups, stirrups are elastic and the compressive stress at the crack interface was on average 2.42 MPa and 4.17 MPa, respectively. This compressive stress slightly increases to 2.73 MPa and 5.74 MPa for the specimens R5 with two and four stirrups, respectively.

For the non-reactive concrete specimens with two stirrups, the average peak aggregate interlock stresses, $v_{ci,peak}$, reached 7.69 MPa compared to 11.25 MPa for the specimens with four stirrup. That increase of aggregate interlock can be attributed to the larger compressive stress on the crack interface for the specimen with four stirrups. The non-reactive concrete specimens with two and four stirrups exhibited similar crack widths at the peak but the specimens with four stirrups experienced a compressive stress on the crack interface about twice as much as the specimens with

two stirrups. These results show that increasing the amount of stirrups increases $f_{ci,peak}$, and hence $v_{ci,peak}$.

Increasing ASR expansion also increases $f_{ci,peak}$ and hence $v_{ci,peak}$. However, yielding of the stirrups also occurs sooner for the reactive concrete specimens and the resulting larger crack tends to reduce $v_{ci,peak}$. These two opposite effects were observed by comparing the specimens with two and four stirrups. For the specimens with two stirrups, increases of w_{peak} of 58% (from 0.19 mm to 0.30 mm, see Table 3) and $f_{ci,peak}$ of 33% were determined for the reactive concrete specimens compared to the non-reactive concrete specimens. This increase results in a peak aggregate interlock increase of 16% on average (from 7.69 MPa to 8.89 MPa) for the reactive concrete specimens compared to the non-reactive concrete specimens. On the contrary, for the reactive concrete specimens with four stirrups (Series 4S), the peak aggregate interlock decreased by 6% on average compared to the non-reactive concrete specimens (from 11.25 MPa to 10.87 MPa). For these reactive concrete specimens with four stirrups, the crack width at the peak increased by 162% (0.15 mm compared to 0.44 mm) while the compressive stress on the crack interface increased by 51% compared to the non-reactive concrete specimens.

Accounting for the microscopic model displayed in Figure 3, expansion increases ASR damage in concrete, which may result in reductions in both mechanical properties and aggregate interlock. The push-off specimens with four stirrups presented higher shear capacities than the specimens with two stirrups. However, for the case of significant ASR-induced expansion, increasing the amount of stirrups results in higher localized stresses on the shear crack interface which tends to give rise to greater strength reductions than the specimens that are not affected by ASR.

6 COMPARISON OF PREDICTIONS WITH PUSH-OFF TEST RESULTS

The aggregate interlock model proposed by Vecchio et al. [18] (Eq. (5)) considers the concrete strength, aggregate size and the crack opening to define the maximum aggregate interlock, $v_{ci,max}$, that can be transmitted across a crack when sufficient stirrups are provided. Increasing the crack width and reducing the aggregate size results in lower values of $v_{ci,max}$. The aggregate interlock shear stress is then determined from the compressive stress on the crack interface, f_{ci}, and the

maximum aggregate interlock, $v_{ci,max}$. When the shear crack runs through the aggregate particles, the aggregate interlock mechanism illustrated in Figure 2 is no longer valid, which may significantly reduce the maximum aggregate interlock, $v_{ci,max}$. In this case, Angelakos et al. [19] suggested using a reduced aggregate size of $a_g = 0$ to determine the maximum aggregate interlock, $v_{ci,max}$. High levels of ASR can result in a similar crack pattern through the aggregate particles (see Figure 3) and a reduced aggregate interlock shear stress. Figure 11 compares the predictions using the Vecchio and Collins model with the push-off test results. For these predictions, the real aggregate size (a_g = 20 mm) and a reduced one for cracks running through the aggregate particles (a_g = 0 mm) were considered to determine $v_{ci,max}$.

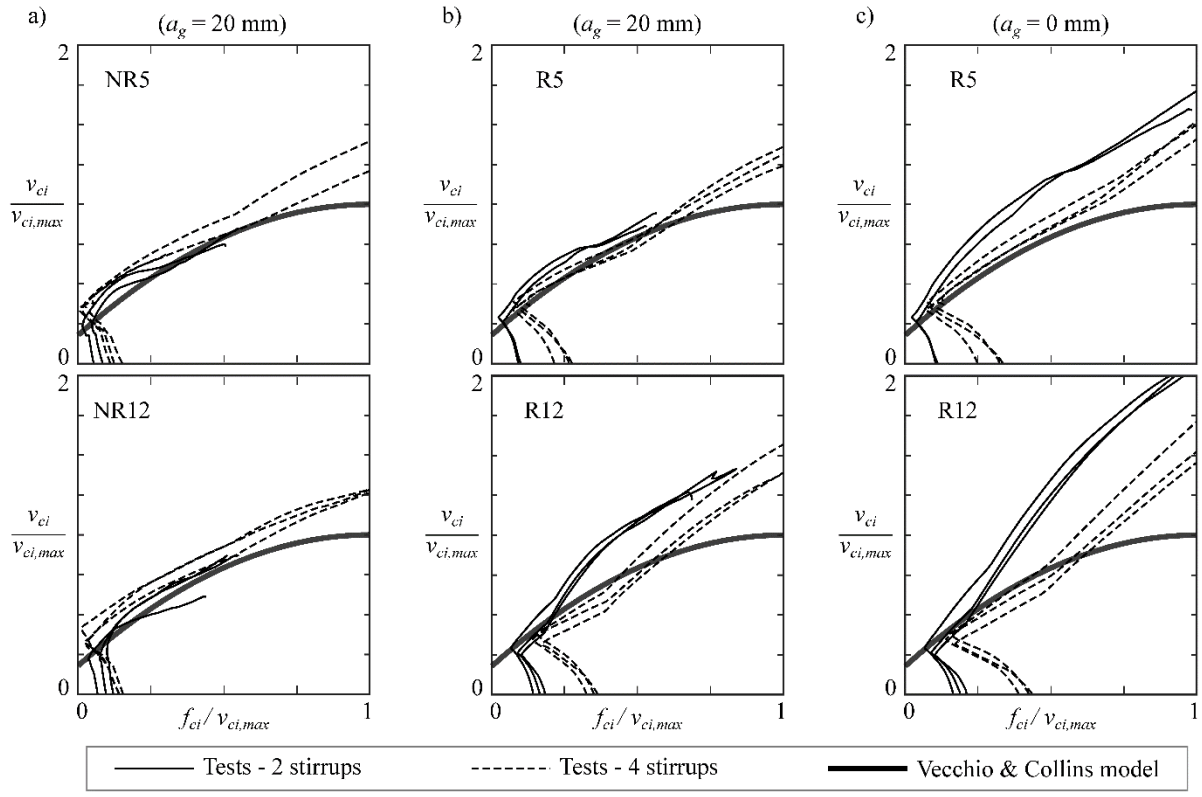

Figure 11: Comparison of predictions using Vecchio et al. [18] model with test results for (a) non-reactive concrete specimens (a_g = 20 mm), (b) reactive concrete specimens considering sound aggregates (a_g = 20 mm) and (c) fractured aggregates (a_g = 0)

The push-off test specimens before any shear is applied have an initial compressive stress across the crack interface, f_{ci}, due to the presence of ASR and the initial cracking along the shear interface (see Figure 11). As shear is applied to a specimen, the crack width and f_{ci} initially decreases as the interlock along the interface starts to be engaged. When the aggregate interlock is engaged, the shear stress ratio reaches the Vecchio et al. [18] model curve, which corresponds to $v_{ci} / v_{ci,max}$ of about 0.18 for the non-reactive concrete specimens. Then, the crack opens and the compressive stress across the crack increases. Increasing the initial prestressing caused by ASR increases the initial ratio $f_{ci} / v_{ci,max}$ so that the crack opening and slippage begin at a shear stress ratio $v_{ci} / v_{ci,max}$ larger than 0.18. The opening of the crack reduces $v_{ci,max}$ and the ratios $v_{ci} / v_{ci,max}$ and $f_{ci} / v_{ci,max}$ increase, even after yielding of the stirrups and after reaching the peak aggregate interlock, $v_{ci,peak}$ (see Figure 9 and Figure 11).

By considering the sound maximum aggregate size (a_g = 20 mm) to determine $v_{ci,max}$, it appears that the Vecchio & Collins model provides a good estimation of the aggregate interlock shear behavior and capacity (see Figure 11). In order to compare the model predictions with the test values for each specimen, the peak value of v_{ci} obtained from the test and the corresponding w and f_{ci} were used in Eq. (5) and (6) to determine the corresponding model peak value. For non-reactive concrete specimens, with 2 stirrups and 4 stirrups, NR5 and NR12, the peak aggregate interlock is slightly underestimated by the model (average model/test value of 0.82, coefficient of variation, CoV, of 6.8%). Very similar peak aggregate interlock underestimation is provided by the model for reactive concrete specimens R5 and R12 when sound aggregates are considered (average model/test value of 0.85, CoV of 10.8%).

By considering fractured aggregates (a_g = 0) to determine $v_{ci,max}$ for reactive concrete specimens, it can be seen from Figure 11c that the predictions using the Vecchio & Collins model gives an overly conservative estimate of the aggregate interlock. On average for reactive concrete specimens R5 and R12, the peak shear stress, $v_{ci,peak}$, determined from the test is 33% larger than the model predictions (average model/test value of 0.67). Furthermore, $v_{ci,peak}$, is underestimated by the model for all the tests and the scattering between experimental tests and Eq. (5) is even

larger for the ASR reactive concrete specimens than for the non-reactive concrete specimens (CoV = 19% for reactive concrete specimens). Hence, it can be concluded that considering fractured aggregates (a_g = 0) in Eq. (5) and (6) is not appropriate for the specimens subjected to ASR expansion levels in this study.

7 CONCLUSIONS:

The main objective of this research was to better understand the influence of ASR on aggregate interlock of reinforced concrete specimens. The main findings are presented here after:

- Confinement due to increased amounts of stirrups delayed the ASR-induced expansion in the direction parallel to the stirrups. However, the confinement did not affect the maximum expansion level reached by the specimens.
- Increasing ASR-induced expansion and the amount of stirrups increases the initial tensile stress in the stirrups and the compressive stress transmitted across the shear crack interface. Consequently, a larger shear must be applied to initiate crack opening and slippage and the stirrups across the shear crack yield at a smaller slip for the ASR-affected concrete specimens.
- After stirrup yielding, the reactive concrete specimens experience larger shear cracks than the non-reactive concrete specimens.
- No significant reduction in aggregate interlock was attributed to ASR-induced damage for the tested specimens subjected to ASR having expansion levels less than about 0.12%.
- There are two opposing effects for ASR-affected concrete: a larger compressive stress across the crack interface increases aggregate interlock while a larger shear crack width reduces aggregate interlock. ASR-affected concrete specimens experience these two opposite effects and aggregate interlock may increase or decrease regarding their relative importance.
- The Vecchio and Collins aggregate interlock model considers these two effects. For the ASR expansion levels studied, this model predicts well the aggregate interlock shear behavior when the real aggregate size is considered. It therefore appears that the potential cracking through the aggregate particles did not progress enough to reduce aggregate resistance and interlock.

ACKNOWLEDGMENTS

The authors gratefully acknowledge the financial support of the Natural Sciences and Engineering Council of Canada in funding the Discovery Grants program and the CREATE program as well as

the support of the *Centre de Recherche sur les Infrastructures en Béton* (CRIB). The authors also acknowledge the input of Professor Benoît Fournier and the laboratory support of Mathieu Thomassin.

REFERENCES:

[1] Sanchez LFM, Fournier B, Jolin M, Mitchell D, Bastien J. Overall assessment of Alkali-Aggregate Reaction (AAR) in concretes presenting different strengths and incorporating a wide range of reactive aggregate types and natures. Cement and Concrete Research. 2017;93:17-31. 10.1016/j.cemconres.2016.12.001

[2] Farny JA, Kerkhoff B. Diagnosis and control of alkali-aggregate reactions in concrete. Skokie, Ill.: Portland Cement Association; 2007.

[3] Fournier B, Berube MA. Alkali-aggregate reaction in concrete: a review of basic concepts and engineering implications. Canadian Journal of Civil Engineering. 2000;27:167-91. 10.1139/l99-072

[4] Kubo MNY. Effect of reactive aggregate on mechanical properties of concrete affected by alkali-silica reaction. 14th International Conference on Alkali–Aggregate Reaction in Concrete. Ausin, Texas2012.

[5] Giaccio G, Zerbino R, Ponce JM, Batic OR. Mechanical behavior of concretes damaged by alkali-silica reaction. Cement and Concrete Research. 2008;38:993-1004. 10.1016/j.cemconres.2008.02.009

[6] Sanchez LFM, Fournier B, Jolin M, Duchesne J. Reliable quantification of AAR damage through assessment of the Damage Rating Index (DRI). Cement and Concrete Research. 2015;67:74-92. 10.1016/j.cemconres.2014.08.002

[7] ASCE-ACI-445. Recent Approaches to Shear Design of Structural Concrete. Journal of Structural Engineering. 1998;124:1375-417. doi:10.1061/(ASCE)0733-9445(1998)124:12(1375)

[8] Rahal KN, Collins MP. Background to the General Method of Shear Design in the 1994 CSA-A23.3 Standard. Canadian Journal of Civil Engineering. 1999;26:827-39. 10.1139/l99-050

[9] Bentz EC, Vecchio FJ, Collins MR. Simplified Modified Compression Field Theory for Calculating Shear Strength of Reinforced Concrete Elements. ACI Structural Journal. 2006;103:614-24.

[10] Muttoni A, Fernández Ruiz M. Shear Strength of Members Without Transverse Reinforcement as Function of Critical Shear Crack Width. ACI Structural Journal. 2008;105:163-72.

[11] Sigrist V, Bentz E, Fernández Ruiz M, Foster S, Muttoni A. Background to the fib Model Code 2010 Shear Provisions – Part I: Beams and Slabs. Structural Concrete. 2013;14:195-203. 10.1002/suco.201200066

[12] Walraven JC. Aggregate Interlock a Theoretical and Experimental Analysis. Delft University Press: Delft University; 1980.

[13] Walraven J, Stroband J. Shear Friction in High-Strength Concrete. ACI special Publication. 1994;149:311-30. 10.14359/4089

[14] Nakarai K, Ogawa Y, Kawai K, Sato R. Shear Strength of Reinforced Limestone Aggregate Concrete Beams. ACI Structural Journal. 2017;114:1007-18. 10.14359/51689725

[15] Sagaseta J, Vollum R. Influence of aggregate fracture on shear transfer through cracks in reinforced concrete. Magazine of Concrete Research. 2011;63:119-37.

[16] Sagaseta J. The influence of aggregate fracture on the shear strength of reinforced concrete beams. London, UK: Imperial College London 2008.

[17] fib. fib Model Code for Concrete Structures 2010. Lausanne, Switzerland: Ernst and Sohn; 2013.

[18] Vecchio FJ, Collins MP. The Modified Compression-Field Theory for Reinforced-Concrete Elements Subjected to Shear. ACI Journal. 1986;83:219-31.

[19] Angelakos D, Bentz EC, Collins MP. Effect of Concrete Strength and Minimum Stirrups on Shear Strength of Large Members. ACI Structural Journal. 2001;98:290-300.

[20] CSA-A23.3. Design of Concrete Structures. Mississauga, Canada: Canadian Standards Association 2019. p. 301.

[21] CSA-S6. Canadian Highway Bridge Design Code and Commentary. 11th ed. Mississauga, Canada: Canadian Standards Association; 2019.

[22] AASHTO. LRFD Bridge Design Specifications 9th Ed. . Washington US: American Association of State Highway and Transportation Officials; 2020.

[23] Blight GE, Alexander MG. Alkali-aggregate reaction and structural damage to concrete: engineering assessment, repair and management. London, UK: CRC Press; 2011.

[24] Duthinh D. Sensitivity of sheer strength of reinforced concrete and prestressed concrete beams to shear friction and concrete softening according to modified compression field theory. Aci Structural Journal. 1999;96:495-508.

[25] Yang KH, Ashour AF. Aggregate interlock in lightweight concrete continuous deep beams. Engineering Structures. 2011;33:136-45. 10.1016/j.engstruct.2010.09.026

[26] Bilodeau S. Étude du comportement structural de dalles épaisses atteintes de la réaction Alcalis-Silice. Québec, Canada: Université Laval; 2017.

[27] Barbosa RA, Hansen KK. Alkali-Silica Reaction in Reinforced Concrete Structures Part II : Shear Strength of Severe ASR Damaged Concrete Beams.1-4.

[28] Jurcut A-C. Modelling of alkali-aggregate reaction effects in reinforced concrete structures. Toronto, Canada: University of Toronto; 2015.

[29] Saouma VE, Hariri-Ardebili MA, Le Pape Y, Balaji R. Effect of alkali–silica reaction on the shear strength of reinforced concrete structural members. A numerical and statistical study. Nuclear Engineering and Design. 2016;310:295-310. https://doi.org/10.1016/j.nucengdes.2016.10.012

[30] Uijl JA, Kaptijn N. Shear tests on beams cut from ASR-affected bridge decks. In: Issa MA, Mo YL, editors. Large-Scale Structural Testing. Farmington Hills: American Concrete Institute; 2003. p. 115-33.

[31] Chana PS, Korobokis GA. Structural performance of reinforced concrete affected by alkali silica reaction. Bridges Division, Structures Group, Transport and Road Research Laboratory; 1991. p. 77.

[32] CSA-G30.18. Carbon steel bars for concrete reinforcement. Mississauga, Canada: CSA; 2009. p. 32.

[33] Fournier B, Ideker JH, Folliard KJ, Thomas MDA, Nkinamubanzi PC, Chevrier R. Effect of environmental conditions on expansion in concrete due to alkali-silica reaction (ASR). Mater Charact. 2009;60:669-79. 10.1016/j.matchar.2008.12.018

[34] ASTM-C1293. Standard Test Method for Determination of Length Change of Concrete Due to Alkali- Silica Reaction. West Conshohocken, PA: ASTM International; 2018. p. 14.

[35] A23.2-14C C. Obtaining and Testing Drilled Cores for Compressive Strength Testing. CSA Group; 2014.

[36] Maekawa K, Qureshi J. Computational model for reinforcing bar embedded in concrete under combined axial pullout and transverse displacement. Materials, Conccrete Structures, Pavements, JSCE. 1996;1996:227-39.

[37] Moradi AR, Soltani M, Tasnimi AA. A Simplified Constitutive Model for Dowel Action across RC Cracks. Journal of Advanced Concrete Technology. 2012;10:264-77. 10.3151/jact.10.264

[38] Moradi AR. Numerical and experimental simulation of dowel action across reinforced concrete (RC) cracks under two-directional loading. Canadian Journal of Civil Engineering. 2018;45:634-46. 10.1139/cjce-2017-0587

[39] Moradi AR, Soltani M, Tasnimi AA. Stress-Transfer Behavior of Reinforced Concrete Cracks and Interfaces. ACI Structural Journal. 2015;112:69-79.

[40] Soltani M, Maekawa K. Path-dependent mechanical model for deformed reinforcing bars at RC interface under coupled cyclic shear and pullout tension. Engineering Structures. 2008;30:1079-91. 10.1016/j.engstruct.2007.06.013

[41] Maekawa K, Qureshi J. Stress transfer across interfaces in reinforced concrete due to aggregate interlock and dowel action. Doboku Gakkai Ronbunshu. 1997;1997:159-72.

[42] Fernández Ruiz M, Muttoni A, Gambarova PG. Analytical Modeling of the Pre- and Postyield Behavior of Bond in Reinforced Concrete. Journal of Structural Engineering. 2007;133:1364-72. 10.1061/(ASCE)0733-9445(2007)133:10(1364)

[43] Fiset M, Villemure F-A, Bastien J, Mitchell D. Behavior of post-installed bonded bars as shear reinforcement. ACI Structural Journal. 2019;117:159-68.

[44] Fiset M. Étude du comportement des éléments en béton armé post-renforcés à l'effort tranchant. Québec: Université Laval; 2019.